 FDMP, vol.3, no.3, pp.231-245, 2007

A Comparative Study of G-jitter Effect on Thermal Diffusion aboard the International Space Station

Y. Yan[1], K. Jules[2] and M. Z. Saghir[1]

Abstract: Fluid science research including thermal diffusion in fluids benefits from the quiescent low-gravity environment provided by the International Space Station (ISS). However, residual gravities (or g-jitters) aboard the ISS impact the overall environment in which experiments are being performed. The impact of these residual gravities needs to be assessed to ensure that they are appropriately accounted for when results are being reported for experiments performed onboard the ISS. In this paper we study the thermal diffusion process in a ternary mixture of n-butane, dodecane and methane. Measured data from the Space Acceleration Measurement System (SAMS) acceleration system onboard the ISS and related influence on fluid flow are compared with the ideal zero-gravity simulation to illustrate the effect of reduced gravity (small accelerations) on thermal diffusion. A three-dimensional numerical model is implemented for the study of various g-jitter scenarios. It is found that the ISS microgravity environment can cause the diffusion process to depart from the ideal behaviour in some circumstances. Such departure varies with the magnitude of the g-jitters and may be insignificant when the g-jitter magnitude is below a threshold value around 10μg. Furthermore, the magnitude of the g-jitters is not the only factor affecting the diffusion process. It has to be evaluated together with the frequency and alignment of the g-jitters. In general, this comparative study indicates that the ISS is an effective reduced gravity platform for experimental diffusion studies.

[1] Ryerson University, Department of Mechanical and Industrial Engineering, 350 Victoria Street, Toronto, ON, M5B 2K3, Canada

[2] NASA Johnson Space Center, Mail Code OZ4, 2101 NASA Parkway, Houston, Texas, USA

Keyword: Thermal diffusion; reduced gravity; G-jitter; Finite volume method; Ternary mixture.

1 Introduction

Thermal diffusion coefficient is a quantity that measures the thermal diffusion process, a phenomenon of a convection-free mixture that separates under a thermal gradient. A precise knowledge of thermal diffusion coefficients is very important in many engineering applications related to mixture separation and mass transport. In the petroleum industry, accurate thermal diffusion coefficients for hydrocarbon mixtures are essential input data in order to have a comprehensive thermodynamic model that can predict the migration and separation of crude oil components under the influence of (ordinary) diffusion, geothermal gradients and gravity field.

Thermal diffusion may be studied theoretically or experimentally. Many models have been developed based on different theories (Dougherty and Drickamer 1955; Bearman *et al*. 1958; Rutherford 1959; Haase 1969; Mortimer and Eyring 1980; López de Haro *et al.* 1983; Kincaid *et al.* 1983; Guy 1986; Kempers 1989; Shukla and Firoozabadi 1998; Firoozabadi *et al*. 2000; Kempers 2001). These models have made significant contribution to the development of the thermal diffusion theories. However, such development is not yet complete and still needs extensive support from experimental studies.

Measurements of thermal diffusion coefficients under terrestrial conditions are very complex due to the strong convection induced by the Earth gravity. Nowadays, free flying platforms such as the ISS are promising and feasible means for conducting diffusion experiments as a result of the reduced gravity environment that they provide. It

has been noted, however, that the residual accelerations or g-jitters in space laboratories may induce convection and thus affect the accuracy of the experiments. Such impact needs to be analyzed in order to make the best use of the space laboratories.

In the literature, the effect of different gravity modulations on thermal diffusion has been investigated numerically through solving either the full Navier-Stokes equations or the time-averaged equations derived from the thermovibrational theory (Gershuni and Lyubimov 1998). The time-averaged technique can produce a fast evaluation of the overall convective effect induced by g-jitters. It is, however, valid only in the high frequency range. Bardan *et al.* (2001) studied the effect of high-frequency vibrations on doubly diffusive convection in square and rectangular enclosures with time-averaged Boussinesq equations and they observed a different effect of vibration on convection according to its direction. The group of Monti, Savino and Lappa (Monti *et al.* 2001; Monti *et al.* 2002; Savino 2002) conducted several studies using the time-averaged technique to simulate fluid experiments in the ISS reduced gravity environment. They pointed out that the convective disturbance can be reduced by orienting the experimental cell such that the g-jitter or the residual-g is parallel to the density gradient. In addition, Savino and Lappa (2003) assessed the thermovibrational theory by evaluating the magnitudes of all the terms in the governing equations. Through an a posteriori analysis of the different diffusive, convective and production terms in the Navier-Stocks equations, they developed a new set of reduced equations for relatively low frequency vibration.

Compared to the time-averaged equations, the solution to the transient Navier-Stokes equations gives the instantaneous flow dynamics. Shu *et al.* (2001) adopted this method in their study of the double diffusion convection in binary alloy melt systems. They found that the increase of g-jitter force (or amplitude) strengthens the nonlinear convective effects, which in turn drastically change the concentration fields. Their simulation for a "real" reduced gravity environment also shows a random response of the velocity and concentration to the g-jitter perturbations. Alexander (1994), by solving the complete set of equations, showed that the orientation of vibrations relative to the density gradient determines whether a mean flow is generated in the system. Chacha *et al.* (2002) and Chacha and Saghir (2005a) conducted studies on thermal diffusion under different gravity modulations by solving the transient Navier-Stokes equations coupled with the mass and heat transfer equations. Their study for a binary system showed that the g-jitter can overcome the Soret effect to a certain degree, and the induced reduction in the component separation is pronounced especially when the g-jitter direction is orthogonal to the density gradient. They also found that the Soret number oscillates with time at the same frequency as the g-jitter excitation. However, the backflow disturbs this variation and makes it non-sinusoidal in shape. Yan *et al.* (2005) and Yan *et al.* (2006) focused on the low frequency g-jitter effect on thermal diffusion. Their numerical results showed that the overall effect of vibrations on diffusion exhibits a characteristic of nonlinearity between each individual effect caused by the g-jitter components; and such nonlinearity is very significant when the g-jitters have low frequency but high amplitude.

A direct numerical simulation of thermal diffusion onboard FOTON-12, a Russian free flyer capsule, was carried out by Chacha and Saghir (2005b). To our best knowledge, this is the only published numerical study concerning ternary mixtures in an actual reduced gravity environment. Their results showed that the diffusion process is slightly affected by the g-jitter onboard the FOTON platform, and such effect is sensitive to the alignment of the fluid cell with respect to the direction of the g-jitter. In a favourable orientation the g-jitter effect on diffusion is negligible. Otherwise, the g-jitter effect is considerable.

In addition, numerous studies have been conducted concerning the thermovibrational convection in general (without thermal diffusion). They may be found in Fu and Shieh (1992), Farooq and Homsy (1996), Lizée and Alexander (1997), Chen and Chen (1999), Hirata *et al.* (2001), Cisse

et al. (2004), Shu *et al.* (2005), Lappa (2005), Okano *et al.* (2006), Kozlov and Selin (2006), Semma *et al.* (2006) to name a few. From the recent literature, it is noticed that the study concerning diffusion process in ternary mixture systems in a reduced gravity is still rare. The main purpose of this paper is thus to investigate the mass-thermo-fluid dynamics of ternary fluid mixtures aboard the ISS. A three dimensional numerical model is implemented in this study, where the full transient Navier-Stocks equations and the energy and mass conservation equations are solved through a finite volume method. Six g-jitter scenarios are investigated, including five sets of measured acceleration data from the SAMS acceleration system onboard the ISS and one ideal theoretical zero-gravity case. By comparing the diffusion process under different g-jitter scenarios, this study also intends to identify the causes of the discrepancy between an actual microgravity environment and the ideal zero gravity environment, which may serve as a scientific guideline to improve the accuracy of space experiments.

2 Three dimensional mathematical model

As shown in Fig. 1, the system consists of a ternary mixture of n-butane, dodecane and methane (0.2/0.3/0.5 mole fraction) in a rectangular cavity (19mm $\times$ 6mm $\times$ 6mm) heated from one side wall. This mixture is one of the typical benchmark fluids in space experiments and also can represent light components in hydrocarbon reservoirs. The cavity is initially homogenous; when the temperature gradient is applied between two side walls, the components of the mixture tend to separate from each other due to the effect of thermal diffusion. Tab. 1 lists the physical properties of the mixture. The system experiences an arbitrary microvibration, which is represented by a gravity vector. The X, Y and Z axes in the model are aligned with the ISS accelerometer data X, Y and Z axes, respectively. Three locations in the X-Z midplane, P1 (x =1.6mm, y =3mm, z =1mm), P2 (x =9.5mm, y =3mm, z =3mm) and P3 (x =17.4mm, y =3mm, z =5mm) will be used in later sections to analyze the results.

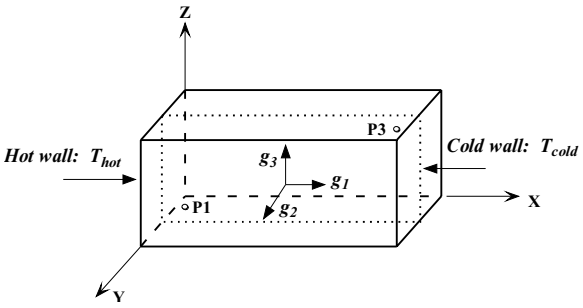

Figure 1: Physical model of the cavity

Table 1: Physical properties of the mixture

T_0	333.15 K
p_0	35 MPa
ρ_0 at (T_0, p_0)	594.39 kg/m3
μ_0 at (T_0, p_0)	2.048×10^{-4} Pa s
c_P	2399.0 J/(kg K)
k	0.1054 W/(m K)
T_{hot}	338.15K
T_{cold}	328.15K

2.1 Governing equations

The physical problem is governed by the continuity, momentum and energy equations; and the principle of species mass conservation (without source terms) is applied to the non-carrier components, c_i (i = 1, 2), respectively, of the mixture. The governing equations in the Cartesian coordinate system are thus given by:

Continuity equation:

$$\frac{\partial \rho}{\partial t} + \nabla \cdot (\rho \vec{\mathbf{u}}) = 0 \tag{1}$$

Species conservation:

$$\frac{\partial}{\partial t}(\rho c_i) + \nabla \cdot (\rho \vec{\mathbf{u}} c_i) = -\nabla \cdot \vec{\mathbf{j}}_i, \quad (i = 1,2) \tag{2}$$

$$\vec{\boldsymbol{j}}_i = -\rho \left(\sum_{j=1}^{2} D_{ij} \nabla c_j + D_{T,i} \nabla T \right), \quad (i = 1,2) \tag{3}$$

Momentum equation:

$$\frac{\partial}{\partial t}(\rho u) + \nabla \cdot (\rho \vec{\mathbf{u}} u) = -\frac{\partial p}{\partial x} + \nabla \cdot (\mu \nabla u) + \rho g_1$$

(4)

$$\frac{\partial}{\partial t}(\rho v)+\nabla\cdot(\rho\vec{\mathbf{u}}v)=-\frac{\partial p}{\partial y}+\nabla\cdot(\mu\nabla v)+\rho g_2 \quad (5)$$

$$\frac{\partial}{\partial t}(\rho w)+\nabla\cdot(\rho\vec{\mathbf{u}}w)=-\frac{\partial p}{\partial z}+\nabla\cdot(\mu\nabla w)+\rho g_3 \quad (6)$$

Energy equation:

$$\frac{\partial}{\partial t}(\rho T)+\nabla\cdot(\rho\vec{\mathbf{u}}T)=\nabla\cdot(k/c_p\nabla T) \quad (7)$$

where $\vec{\mathbf{u}}$ is the velocity vector, $\vec{\mathbf{u}}=u\vec{i}+v\vec{j}+w\vec{k}$; ρ is the density; μ is the dynamic viscosity; t denotes the time; $\vec{\mathbf{j}}_i$, D_{ij} and $D_{T,i}$ are the diffusion flux, molecular diffusion coefficient and thermal diffusion coefficient, respectively. The thermal diffusion coefficient uses the definition in Firoozabadi *et al.* (2000). g_1, g_2 and g_3 represent the g-jitters in X, Y, and Z directions, respectively, see eq.14 in section 3. In addition, the Peng-Robinson equation of state (Peng and Robison 1976; Twu *et al.* 1995) is used for the density.

2.2 Boundary and initial conditions

Three assumptions are applied to the system: (1) the walls are rigid and there is no flow and no slip; (2) the walls are adiabatic, except the two opposite side walls which are in constant temperatures; and (3) there is no reaction inside the cavity and no mass flux through the cavity walls. Therefore the boundary conditions for the velocity, temperature and diffusion flux are given by:

Velocity: $\vec{\mathbf{u}}=0$ (8)

Diffusion flux: $\vec{\mathbf{j}}_i=0, \quad (i=1,2)$ (9)

Temperature: $T|_{x=0}=T_{hot}, \quad T|_{x=L}=T_{cold}$

$$\left.\frac{\partial T}{\partial y}\right|_{y=0,y=W}=0, \quad \left.\frac{\partial T}{\partial z}\right|_{z=0,z=H}=0 \quad (10)$$

The initial conditions are $\vec{\mathbf{u}}_0=0$, $p_0=35MPa$ and $T_0=333.15K$ $(0<x<L)$.

2.3 Numerical method

Equations 1-10 contain eight unknowns u, v, w, ρ, p, T, c_1, c_2 to be solved for each mesh point in the cavity. The SIMPLE algorithm (Patankar 1980) is employed in our model, which uses the finite volume method to discretize the governing equations. In this algorithm, the pressure and velocity fields consist of two components: an approximate field (p^* or $\vec{\mathbf{u}}^*$) and a correction field (p' or $\vec{\mathbf{u}}'$), as follows:

$$p=p^*+p', \quad \vec{\mathbf{u}}=\vec{\mathbf{u}}^*+\vec{\mathbf{u}}' \quad (11)$$

The velocity correction $\vec{\mathbf{u}}'$ and the pressure correction p' are related through Eq. 12:

$$\vec{\mathbf{u}}'=-K\cdot\nabla p', \quad K=\begin{pmatrix}K_x & 0 & 0\\ 0 & K_y & 0\\ 0 & 0 & K_z\end{pmatrix} \quad (12)$$

where K is a diagonal tensor resulting from the discretization scheme. First, the discretized momentum equation is solved to obtain $\vec{\mathbf{u}}^*$ through p^*; and then by solving the continuity Eq. 1 with Eqs 11 and 12, the pressure correction field p' is obtained as given by Eq.13. This pressure correction is then used to update the velocity and pressure field.

$$\frac{\partial\rho}{\partial t}+\nabla\cdot(\rho\vec{\mathbf{u}}^*)=\nabla\cdot(\rho K\cdot\nabla p') \quad (13)$$

The solution proceeds via a decoupled iterative solver, NSPCG (Non-Symmetric Preconditioned Conjugate Gradient) package, until for each time step the convergence is achieved, i.e., the maximum relative error for the unknown variables between two successive iterations is less than 10^{-6}.

Physically unrealistic solutions are avoided through the use of a power-law scheme, which provides a good approximation of the convection and diffusion terms even for coarse grids. The time discretization uses a first-order, fully implicit scheme. In addition, the numerical model uses a staggered, non-overlapping, rectangular grid system. The velocity components are defined at the grid faces whereas the pressure, temperature and species concentrations are calculated at the center of the grids. Details of the numerical procedure

may be found in Chacha *et al.* (2003). The molecular and thermal diffusion coefficients are calculated as a function of the temperature and component concentrations according to Firoozabadi *et al.* (2000).

Table 2: Optimal mesh analysis

Mesh size	Nu_{hot}	CPU time*(seconds)
11×11×11	3.171	3717
21×11×11	3.228	2735
31×11×11	**3.109**	**6603**
41×11×11	3.060	8918
61×11×11	3.025	25208
21×21×21	3.189	39422
61×21×21	2.988	1079970

* Total CPU time consumption needed to reach quasi steady state

A validation of the numerical code was shown in previous studies (Chacha *et al.* 2003, Chacha and Saghir 2005a, Chacha and Saghir 2005b, Yan *et al.* 2005 and Yan *et al.* 2006). A mesh sensitivity analysis has been conducted based on the Nusselt number at the hot wall (Chacha *et al.* 2003). Since g-jitter magnitudes in most reduced gravity environments are smaller than 10000μg (10^{-2}g), in this study the static 10000μg has been considered as the reference case for the optimal mesh analysis. Tab. 2 shows the results. It is noted that the mesh size along the X direction is of great importance to the accuracy of the results. By considering the Nusselt number and the CPU time needed for the computation, the optimal mesh is found to be $31 \times 11 \times 11$, which gives only 4% of difference in Nusselt number but saves (162 times) time compared to a much finer mesh 61×21×21.

3 G-jitter data measurement onboard the ISS and processing

As explained before, one of the major goals of the ISS is to provide a quiescent low-gravity environment to perform fundamental scientific research. However, small disturbances aboard the Space Station impact the overall environment in which experiments are being performed. Such small disturbances need to be measured in order to assess their potential impact on the experiments. In order to accomplish that, NASA developed and installed two accelerometer systems onboard the ISS to acquire such measurements. For this comparative study, the acceleration data measured by SAMS onboard the ISS are used. SAMS measures the vibratory/transient accelerations caused by vehicle, crew, and experiment disturbances, which occur in the frequency range of 0.01 to 400 Hz. SAMS is distributed across the U.S Destiny module (U.S science module). For this study, in particular the data from two SAMS Sensor Enclosure (SE) heads are used: 121f02 and 121f04. SAMS SE 121f02 was mounted in the SAMS International Subrack Interface Standard (ISIS) drawer 1 in the Expedite the Processing of Experiments to the Space Station (EXPRESS) Rack 1; while SAMS SE 121f04 was mounted on the lower Z Panel assembly below EXPRESS Rack 1, see Fig. 2. This means that SE 121f02 was located inside a drawer in EXPRESS Rack 1; while SE 121f04 was mounted in-between the lower part of the rack (at the bottom of the rack) and the ISS structure. Therefore, SE 121f04 measured directly what the ISS structure was experiencing, in terms of excitation/vibration, at that specific location; while SE 121f02 measured what the rack, at the drawer location, was experiencing. Each sensor head has a defined coordinate system whose location and orientation are given with respect to the Space Station Analysis Coordinate System. The origin is defined as the triaxial center point of the three accelerometers that comprise the head.

The acceleration data measured by the SAMS SE 121f02 was collected at 100 Hz; while SE 121f04's was collected at 200 Hz. However, since a fluid tends to respond to much lower frequencies, both SE 121f02 and 121f04 acceleration data collected at the 100 and 200 Hz were low-pass filtered to 6 Hz, effectively removing the high frequency/energy content of the signal. The actual frequency band of interest for this study is 2 Hz; therefore only data with frequency lower than 2 Hz have been used. Also, since we are interested only in the oscillatory components, steady residual g contributions have not been considered.

This study addresses several scenarios using the

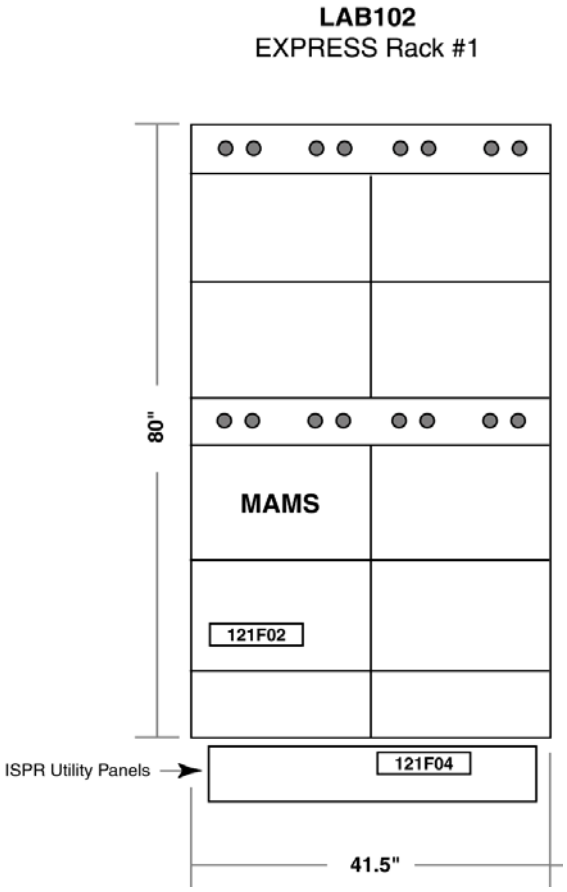

Figure 2: MAMS and SAMS (Sensor Enclosure) Locations in the EXPRESS Rack 1 (LAB1O2)

aforementioned actual acceleration data measured aboard the ISS. First, two different accelerometer heads, SE 121f02 and SE 121f04, located at two different locations are used since experiments can be mounted directly to the ISS structure (in a non-isolated mode) or mounted inside a rack, which interfaces with the ISS structure. Second, the attitude Local Vertical Local Horizontal (LVLH) is studied. This is one of the main attitudes flown by ISS. It is well known that the reduced-gravity environment onboard the ISS is significantly affected by the attitude being flown. In fact, there is an increase in acceleration levels due to an increase in gimbal motion, which is required for ISS to track the communication satellites while in an LVLH attitude, for example. Third, acceleration data are considered for two different crew states: (1) when the crew was asleep to remove the impact of crew motion from the acceleration data and (2) when the crew was awake. This is important since science is performed 24-hour and every day on the station (some experiments require crew participation, others are controlled from the ground, with no crew participation). Finally, acceleration data represent two possible conditions: (1) best, the acceleration data measured during the period of time under consideration were plotted into minimum and maximum acceleration magnitude for the conditions defined above. When the acceleration magnitude onboard the ISS was at a minimum throughout, that set of data was labeled "best condition" and (2) worst, when the acceleration magnitude was the maximum. These two conditions (best and worst) define a performance band of the acceleration magnitude onboard the ISS during the time period the data were collected. The acceleration data used in this study covered a period of 6 hours.

In the following, five sets of measured g-jitter acceleration data onboard the ISS are compared with a simulated theoretical zero-gravity case. The measured data represents actual condition onboard the ISS, whereas the simulated theoretical case represents the ideal orbital science platform. Hereafter, these cases are referred to as 121f02_lvlh_sleep_best, 121f02_lvlh_sleep_worst, 121f02_lvlh_wake_best, 121f02_lvlh_wake_worst and 121f04_lvlh_wake_worst with respect to two different crew states and two different locations. The measured g-jitter data have been decomposed to generate the Fourier coefficients, thus the g-jitter vectors may be expressed in Fourier series as follows:

$$g_i(t) = a_i^0 + \sum_{j=1}^{n} \left(a_i^j \cos\left(2\pi f_i^j t\right) + b_i^j \sin\left(2\pi f_i^j t\right) \right) \tag{14}$$

where $i = 1,2,3$ represents the X, Y, and Z directions, respectively; a_i^0, a_i^j and b_i^j $(j = 1,n)$ are the Fourier coefficients; and f_i^j $(j = 1,n)$ is the frequency. It should be pointed out that the g-jitter in each direction consists of a series of harmonic vibrations with the frequencies, $f_i^j = j \cdot f_0$

$(j = 1, n)$, where the fundamental frequency $f_0 = 4.577 \times 10^{-5}$Hz.

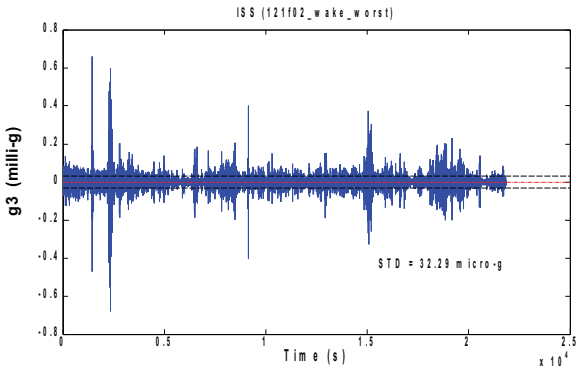

Figure 3: G-jitter data (z-direction) on the ISS. Case: 121f02_lvlh_wake_worst.

Fig. 3 illustrates the random nature of typical g-jitter data measured onboard the ISS. Tab. 3 analyzes the measured g-jitter data to be used in the next section. It is noticed that, in general, g-jitters in Z direction have the largest magnitude according to the standard deviation (STD) with respect to the mean value $\overline{g} = 0$. It is calculated as follows:

$$\mathbf{STD} = \left[\frac{1}{n}\sum_{j=1}^{n}(g_j - \overline{g})^2\right]^{0.5} \tag{15}$$

where n is the total number of g-jitter data samples. Therefore, the temperature gradient is aligned perpendicular to the g-jitter in Z direction to illustrate the possible maximum effect of the reduced gravity environment on diffusion.

Table 3: Statistic analysis for the measured g-jitter data

Case scenario	121f02_lvlh_sleep_best		
	g_1	g_2	g_3
STD (μg)	4.57	6.53	8.86
Min (μg)	-149.61	-183.78	-264.23
Max (μg)	117.99	190.10	269.98
Case scenario	121f02_lvlh_sleep_worst		
	g_1	g_2	g_3
STD (μg)	5.27	6.96	10.31
Min (μg)	-106.18	-148.58	-237.40
Max (μg)	102.39	120.62	214.02
Case scenario	121f02_lvlh_wake_best		
	g_1	g_2	g_3
STD (μg)	6.93	9.13	12.08
Min (μg)	-144.96	-157.57	-175.08
Max (μg)	172.67	203.11	171.38
Case scenario	121f02_lvlh_wake_worst		
	g_1	g_2	g_3
STD (μg)	19.02	27.93	32.29
Min (μg)	-472.35	-730.67	-680.34
Max (μg)	442.67	717.96	660.87
Case scenario	121f04_lvlh_wake_worst		
	g_1	g_2	g_3
STD (μg)	17.44	25.07	36.78
Min (μg)	-346.86	-847.59	-675.24
Max (μg)	401.68	798.11	730.71

4 Results and discussion

4.1 Velocity field

Contrary to the stagnant status at zero-gravity, a singular convective cell is observed in the X-Z midplane in all g-jitter cases (graph not shown). This convective flow accelerates the heat and mass transfer simultaneously and disturbs the component separation process. The strength of such convection varies with time in responding to the g-jitter excitation in each individual case. Fig. 4 shows the velocities for the case 121f02_lvlh_wake_worst when the system approaches the quasi steady state. The irregular shape of the velocities reflects the nature of g-jitters. The Z direction experiences the strongest convection due to the largest g-jitter magnitude as analyzed in Tab. 3. On the contrary, the X direction shows the weakest convection thanks to the smallest g-jitter magnitude and the orientation of the temperature gradient along this direction. The same tendency is also observed in other g-jitter cases. In the following discussions, the X-Z midplane is therefore chosen to discuss the results.

4.2 Temperature profile

In all g-jitter cases, small deviations from the zero-gravity linear distribution are observed in temperature profiles due to the effect of convection. Such deviations may be evaluated through

the maximum temperature deviation, $\delta T_{\max}$, and its mean value, δT_{mean} , during a time interval (t_1, t_2) as defined in Eqs 16 and 17.

$$\delta T_{\max} = \max\left[abs\left(T - T_{linear}\right)\right] \tag{16}$$

$$\delta T_{mean} = \left(\int_{t_1}^{t_2} \delta T_{\max} dt\right) \Big/ \left(t_2 - t_1\right) \tag{17}$$

where T is the local temperature at each mesh node and T_{linear} is the zero-gravity temperature at the same node (purely diffusive ideal condition).

Tab. 4 lists $\delta T_{\max}$ and δT_{mean} for different g-jitter cases during a period of 30 to 40 minutes when the system approaches the quasi steady state. It is noted that the temperature deviation from linear is generally negligible for these cases thanks to their small g-jitter magnitudes. Under such conditions, the heat transfer process is rarely affected thus resulting in those nearly linear temperature profiles. The temperature deviation in these cases increases in the order 121f02_lvlh_sleep_best, 121f02_lvlh_sleep_worst, 121f02_lvlh_wake_best, 121f02_lvlh_wake_worst and 121f04_lvlh_wake_worst indicating the increased effect of convection on temperature as the g-jitter magnitude increases. It is also noted, by comparing the two cases 121f04_lvlh_wake_worst and 121f02_lvlh_wake_worst, that the two environments 121f02 and 121f04 have a similar effect on the temperature distribution inside the experiment cell. This can be very well understood by examining their g-jitter levels as shown in Tab. 3.

Table 4: Temperature deviation from linear distribution

Case scenario	$\delta T_{\max}$ (10^{-3}K)	δT_{mean} (10^{-3}K)
121f02_lvlh_sleep_best	0.15 – 8K	2.5
121f02_lvlh_sleep_worst	0.2 – 12	3
121f02_lvlh_wake_best	0.3 – 28	3.6
121f02_lvlh_wake_worst	1.5 – 32	11
121f04_lvlh_wake_worst	1.8 – 53	14

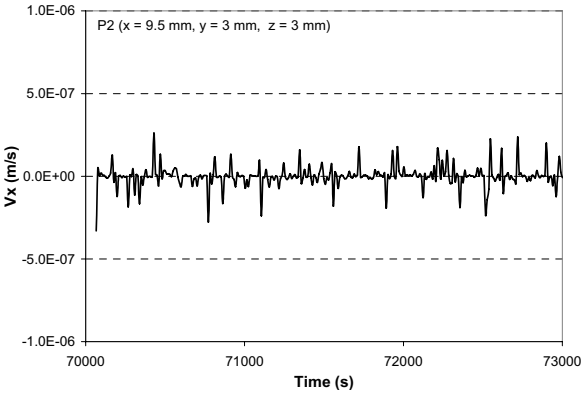

(a) Velocity in the X direction

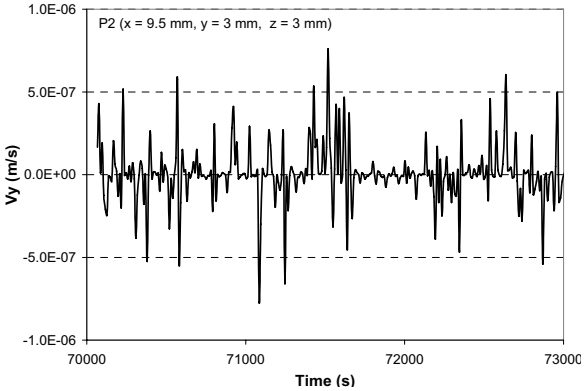

(b) Velocity in the Y direction

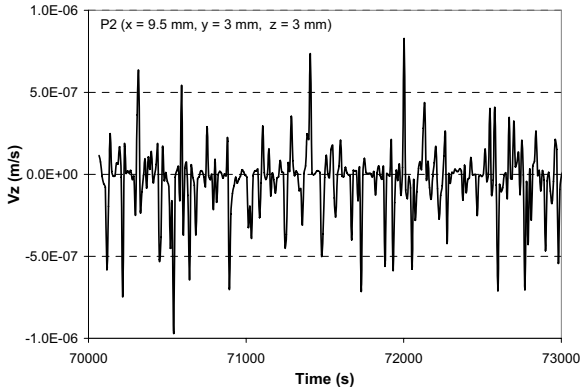

(c) Velocity in the Z direction

Figure 4: Velocity variation in time (case: 121f02_lvlh_wake_worst)

4.3 Component distribution

A component separation is observed under the applied lateral temperature gradient. Dodecane and n-butane being the heavier components migrate to the cold wall; and methane being the lightest

Table 5: Mass density deviation with respect to the linear distribution at zero gravity

Case scenario	At the hot wall	At the cold wall
121f02_lvlh_sleep_best	0.010%	-0.007%
121f02_lvlh_sleep_worst	0.010%	-0.008%
121f02_lvlh_wake_best	0.009%	-0.012%
121f02_lvlh_wake_worst	0.055%	-0.048%
121f04_lvlh_wake_worst	0.048%	-0.046%

component migrates to the hot wall. This component separation causes a non-uniform mixture mass density in the cavity. Ideally at zero gravity, the mixture mass density varies linearly along the X axis. This linear distribution is, however, deformed at the reduced gravity environment due to g-jitters. Fig. 5 compares the mass density distribution for the case 121f02_lvlh_wake_worst with that in zero gravity. It is noted that the deformation in mass density varies with location with the cold and hot walls having the largest deviations. The deviations at the centre points of the hot and cold walls are listed in Tab. 5, which shows that the deformation also increases with the g-jitter magnitude. For the worst scenario, 121f02_lvlh_wake_worst and 121f04_lvlh_wake_worst, the mass density deviation from linear becomes several times larger than that in the best scenario, 121f02_lvlh_sleep_best. These deviations, however, are still very small in general and may be difficult to detect in real experiments. The overall effect of the environments 121f02 and 121f04 on the component distribution is found to be comparable in degree. To further verify this observation, the evolution of the component concentration with time was compared for the g-jitter cases and the ideal zero-gravity case. Fig. 6 shows the comparison for n-butane at the location P1 as an example. The concentration oscillation is obvious throughout the time evolution for all g-jitter cases. It is particularly significant for the worst cases 121f02_lvlh_wake_worst and 121f04_lvlh_wake_worst. Similar behaviours are observed in these two cases and the local oscillations are apparently in corresponding to different local excitations with time. When the system reaches the quasi steady state after about 19 hours, the deviation of the component concentration from its zero-gravity values tends to stabilize. For n-butane at the quasi steady state, for example, the deviation at the location P1 is 0.04% and 0.2% at the best and worst g-jitter scenarios, respectively. Such deviation confirms that the component separation is, indeed, reduced as a result of g-jitters. The degree of this reduction is, however, within a tolerable range.

Fig. 6 shows that, during the time evolution, some time intervals (hereafter referred to as regions) have much stronger oscillations than others. It is therefore interesting to track down the g-jitter magnitude that corresponds to the threshold of large deviations. Figs. 7 and 8 show the results for 121f02_lvlh_wake_best and 121f02_lvlh_wake_worst cases, respectively. It is clearly seen from Fig. 7 that the regions "A" exhibit nearly negligible oscillations; while in the regions "B", the oscillations become noticeable. The average g-jitter magnitudes (absolute values) in the regions "A" and "B" are about 3.8μg and 9.6μg, respectively. On the contrary, the case 121f02_lvlh_wake_worst has much larger oscillations, as shown in Fig. 8. In this case, the g-jitters are more stable and higher in magnitude with an average (absolute value) of 20μg. Results from these analyses may suggest that the threshold of the g-jitter is around 10μg. Above this acceleration level, the g-jitter effect becomes considerable.

4.4 Diffusion coefficients

Molecular and thermal diffusion coefficients are functions of local temperature, pressure and component concentrations. The g-jitter induced convection, by affecting the local parameters, affects the local molecular and thermal diffusion coefficients. Therefore, these diffusion coefficients exhibit oscillations locally. The hot and cold walls are generally affected the most; at the centre of the cavity, the diffusion coefficients slightly oscillate with time. Fig. 9, for example, shows the oscillations of dodecane thermal diffusion coefficient at the location P1 near the hot wall. It is clear that with the existence of g-jitters, the dode-

cane thermal diffusion coefficient has a tendency to deviate from its theoretical zero-gravity value; and as the g-jitter magnitude increases, this tendency becomes very evident, as shown in the case 121f02_lvlh_wake_worst. A similar behaviour is also found in the case 121f04_lvlh_wake_worst, see Fig. 10. The degree of these deviations depends on the intensity of the convection. A detailed evaluation of these deviations is shown in Tab. 6 for the location P1 at the quasi steady state. The sign "-" indicates that near the hot wall the molecular and thermal diffusion coefficients are smaller than their theoretical zero-gravity values. It should be mentioned that, on the contrary, the diffusion coefficients near the cold wall have a tendency to increase from their theoretical zero-gravity values. It is clear, from Tab. 6, that the deviations of diffusion coefficients are generally very small since local parameters vary slightly from their ideal behaviours as discussed in earlier sections. The n-butane thermal diffusion coefficient is an exception; it is very sensitive to g-jitters. This sensitivity may be attributed to its small value at the specified condition (one order smaller than the dodecane thermal diffusion coefficient). As a result, this coefficient may be difficult to measure accurately in comparison to the other coefficients in actual experiments. Therefore, one must exercise caution when measuring it.

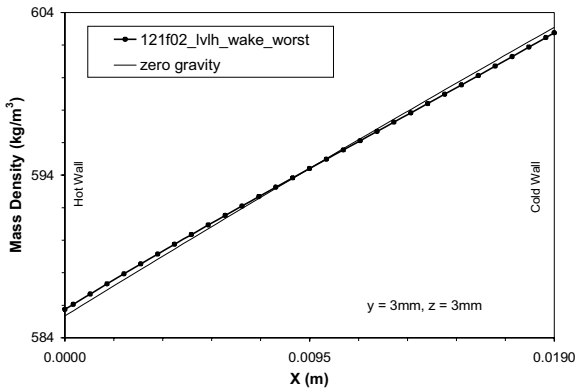

Figure 5: Mass density variation in the X-Z midplane

From Figs. 6, 8 and 9, it is noticed that a sudden increase in g-jitter (e.g., at around 46000 seconds in the case 121f02_lvlh_wake_worst) may cause the system to depart significantly from its ideal zero-gravity behaviour. To further evaluate the effect of g-jitters, particularly for a large g-jitter disturbance on the system at the quasi steady state, a simulation was performed for 121f02_lvlh_wake_worst with the following procedure: a static g-jitter, 600μg, is artificially imposed on the system for a period of 40 seconds after the system reaches the quasi steady state; then the g-jitter is reverted to its normal level and the simulation proceeds until the system returns to the quasi steady state. Fig. 11 shows clearly that the system equilibrium was interrupted due to the imposed large g-jitter, as seen in curve "A". When the g-jitter returns to its normal level, the system gradually approaches the equilibrium status, see curve "B". However, this process is very slow. It takes more than one hour, i.e., 95 times longer than the period during which the system was interrupted. This result indicates that a sudden large disturbance at the quasi steady state can affect the duration and stability of the system equilibrium thus leading to a prolonged experimental time or even worse to the failure of the experiment. It is therefore very important to have strategies for the control of g-jitter magnitudes especially when the system approaches the quasi steady state.

5 Conclusions

In this paper, a zero-g simulation of the diffusion process for a ternary mixture of n-butane, dodecane and methane (0.2/0.3/0.5 mole fraction) has been compared with actual acceleration data measured onboard the ISS to assess the impact of its microgravity environment on potential diffusion experiments. Different g-jitter scenarios with respect to the crew active/inactive have been investigated. It has been found that the diffusion process is negatively affected; the degree of this effect, however, varies depending on the magnitude of the g-jitters. Local oscillations are observed for all cases investigated in terms of the component concentration, velocity, temperature and diffusion coefficients. At the quasi steady state, these local parameters show deviations from their ideal zero-gravity values, but to an insignif-

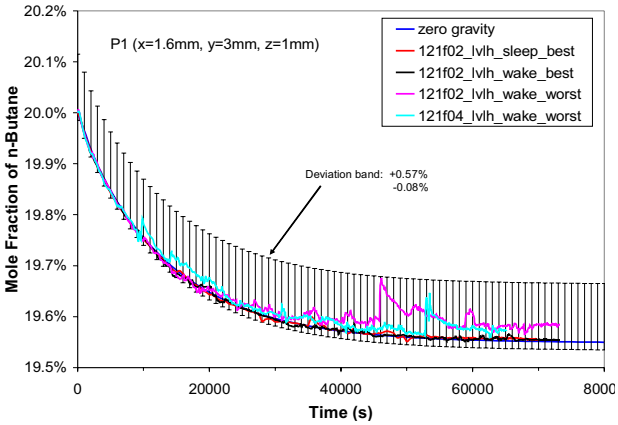

Figure 6: Evolution of n-butane with time at the location P1

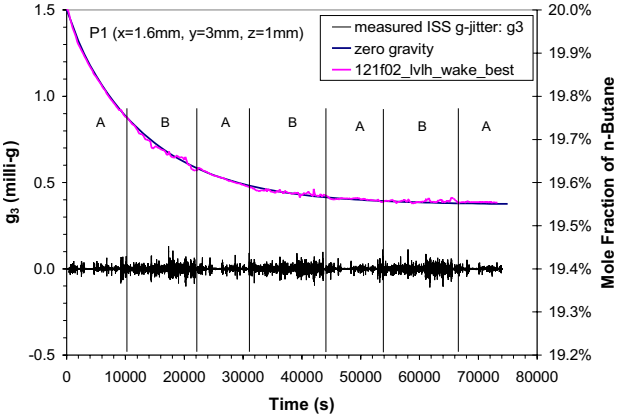

Figure 7: G-jitter threshold analysis for the case "121f02_lvlh_wake_best"

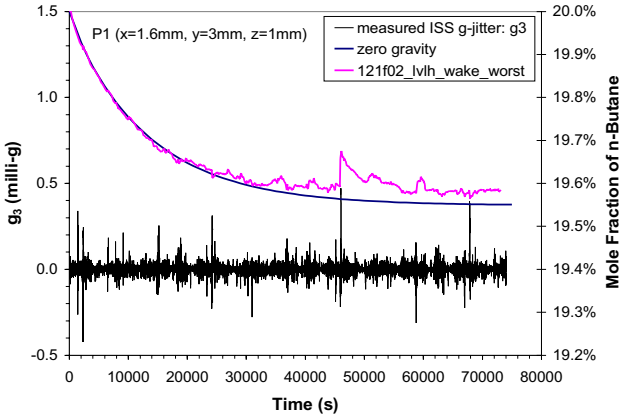

Figure 8: G-jitter threshold analysis for the case "121f02_lvlh_wake_worst"

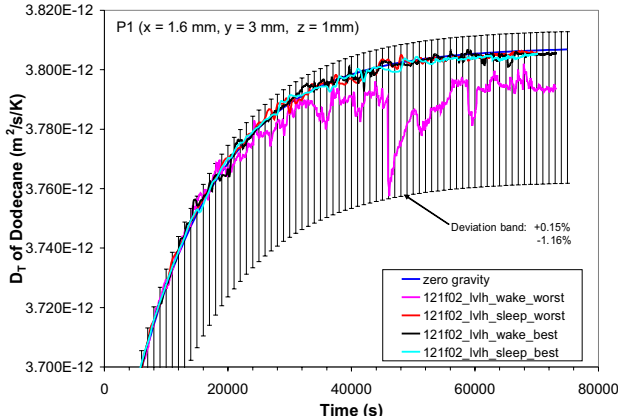

Figure 9: Evolution of dodecane thermal diffusion coefficient with time near the hot wall

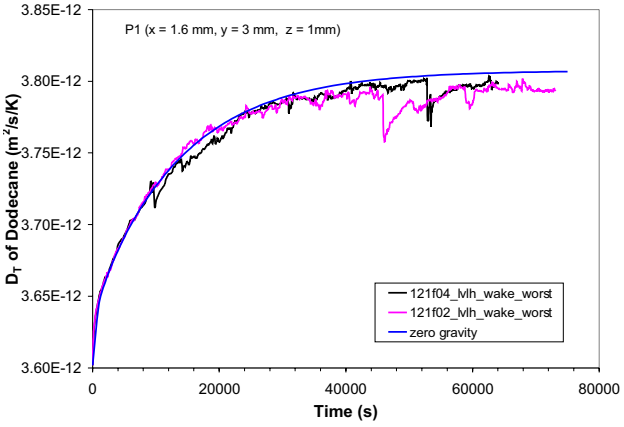

Figure 10: Dodecane thermal diffusion coefficient at two environments 121f02 and 121f04 near the hot wall

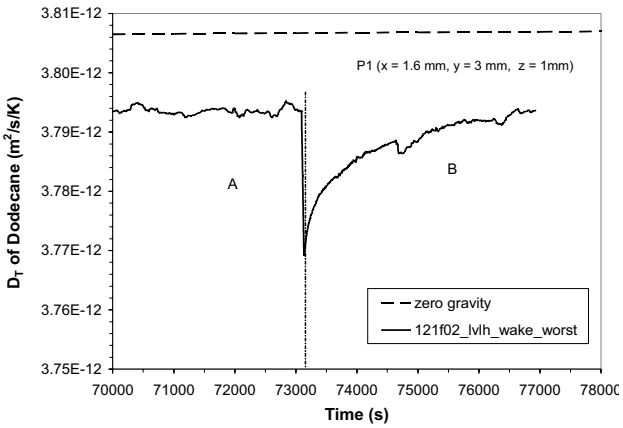

Figure 11: Effect of the sudden jump of g-jitter on diffusion at the quasi steady state

Table 6: Average deviations of diffusion coefficients from 0-g values at the quasi steady state (location: P1)

Case scenario	Molecular diffusion coefficient		Thermal diffusion coefficient	
	Dodecane	n-Butane	Dodecane	n-Butane
121f02_lvlh_sleep_ best	-0.004%	-0.013%	-0.018%	-0.14%
121f02_lvlh_sleep_ worst	-0.007%	-0.026%	-0.036%	-0.27%
121f02_lvlh_wake_ best	-0.015%	-0.045%	-0.058%	-0.45%
121f02_lvlh_wake_ worst	-0.078%	-0.273%	-0.375%	-2.83%
121f04_lvlh_wake_ worst	-0.079%	-0.275%	-0.377%	-2.84%

Table 7: Effect of g-jitters on diffusion

Influential Factors	Findings	References
Magnitude	There exists a threshold magnitude to trigger large deviations from ideal zero-gravity behaviour. It is around 10μg for the cases studied.	this study
	The increase of g-jitter magnitude strengthens the nonlinear convective effects	Shu et al. (2001)
	Increasing the g-jitter magnitude enhances the mixing of the fluid and therefore reduces species differentiation	Chacha and Saghir (2005)
Frequency	The effect of g-jitters on diffusion increases with the decrease of the frequency and the increase of the magnitude. The nonlinear convective effects are very significant when the g-jitters have low frequency but high amplitude.	Yan et al. (2005); Yan et al. (2006)
Alignment	The experimental cell should be oriented in such a way that the g-jitters are parallel to the density gradient (temperature gradient).	Monti et al. (2001); Monti et al. (2002); Savino (2002); Alexander (1994); Chacha and Saghir (2005)

icant degree. Similar behaviours are found for the two environments 121f02 and 121f04, which represent the situations where the experiments are mounted inside a rack or to the ISS structure, respectively. This study reveals that diffusion experiments aboard the ISS can achieve relatively good accuracy. However, to ensure the accuracy, proper control of the g-jitter magnitudes is of great importance. A threshold value of about 10μg seems to be the trigger point above which experiments can be negatively impacted by the environment. In addition, cautions must be taken to maintain the stability of the system equilibrium especially when it approaches the quasi steady state. It is also worth noting that the g-jitter magnitude is not the only influential factor on the accuracy of the results of the experiments. Frequency and alignment of the experimental cell are of equal importance to the fluid science experiments.

Acknowledgement: The authors wish to thank the Canadian Space Agency (CSA) and the National Research and Engineering Council (NSERC) for sponsoring this project.

Nomenclature

a_i^0 Fourier coefficients (j =1,n, i=1,2,3)
a_i^j Fourier coefficients (j =1,n, i=1,2,3)
b_i^j Fourier coefficients (j =1,n, i=1,2,3)
c_i Mixture component Concentration (i = 1, 2)
c_p Specific heat
D_{ij} Molecular diffusion coefficient (i=1,2, j=1,2)
$D_{T,i}$ Thermal diffusion coefficient (i = 1, 2)

f_0	Fundamental frequency in the Fourier series
f_i^j	Frequency (j =1,n, i=1,2,3)
g_i	G-jitter (i=1,2,3 represents the X, Y, and Z directions, respectively)
$\vec{\mathbf{j}}_i$	Diffusion flux, (i = 1, 2)
k	Thermal conductivity
$\mathbf{K}$	Diagonal tensor resulting from the discretization scheme
L	Length of the cavity
p	pressure
T	Temperature
T_{linear}	Linear temperature distribution at 0-g condition
t	Time
u	Velocity in the X direction
$\vec{\mathbf{u}}$	Velocity vector, $\vec{\mathbf{u}} = u\vec{i} + v\vec{j} + w\vec{k}$
v	Velocity in the Y direction
w	Velocity in the Z direction
ρ	Density
μ	Dynamic viscosity
$\delta T_{\max}$	Maximum temperature deviation from linear
δT_{mean}	Mean value of $\delta T_{\max}$ during a time interval

Subscripts

$_0$	reference state or initial state
$_{cold}$	at the cold wall
$_{hot}$	at the hot wall
$_x$	in the X direction
$_y$	in the Y direction
$_z$	in the Z direction

Abbreviations

EOS	Equation of State
EXPRESS	EXpedite the PRocessing of Experiments to the Space Station
ISIS	International Subrack Interface Standard
SAMS	Space Acceleration Measurement System
SE	Sensor Enclosure
STD	Standard Deviation
ISS	International Space Station

References

Alexander J.I.D. (1994). Residual gravity jitter effects on fluid processes, *Microgravity Science and Technology*, vol. 7, pp.131-137

Bardan G., Knobloch E., Mojtabi A., Khallouf H. (2001). Natural doubly diffusive convection with vibration, *Fluid Dynamics Research*, vol. 28, pp.159-187

Bearman, R. J., Kirkwood, J. G., Fixman, M. (1958). *Advances in Chemical Physics*, vol.1, pp.1-13, Interscience Publishers, Inc.: New York

Chacha M., Faruque D., Saghir M.Z., Legros J.C., (2002). Solutal thermodiffusion in binary mixture in the presence of g-jitter, *Int. J. Thermal Science*, vol. 41(**??**), pp.899-911

Chacha M., Saghir M.Z., Van Vaerenbergh S., Legros J.C., (2003). Influence of thermal boundary conditions on the double-diffusive process in a binary mixture, *Philosophical Magazine*, vol. 83(17-18), pp.2109-2129

Chacha M., Saghir M.Z. (2005). Solutal-thermo-diffusion convection in a vibrating rectangular cavity, *Int. J. Thermal Sciences*, vol.44, pp.1-10

Chacha M., Saghir M. Z., Viviani A, (2005). 3D Numerical Simulations of Thermodiffusion Experiment for a Ternary Mixture On-Board Foton, *Microgravity science and technology*, XVII-2, pp.31-37

Chen W.-Y., Chen C. F. (1999). Effect of gravity modulation on the stability of convection in a vertical slot, *J. Fluid Mech.*, vol. 395, pp.327-344

Cisse I., Bardan G., Mojtabi A., (2004). Rayleigh Bénard convective instability of a fluid under high-frequency vibration, *Int. J. Heat Mass Transfer*, vol. 47(19-20), pp 4101-4112

Dougherty, E. L., Drickamer, H. G., (1955). Thermal Diffusion and Molecular Motion in Liquids, *Journal of Physical Chemistry*, vol. 59(5), 443-449

Farooq, A., Homsy, G. M., (1996). Linear and non-linear dynamics of a differentially heated slot under gravity modulation, *J. Fluid Mech.*, vol. 313, pp.1-38

Firoozabadi, A., Ghorayeb, K., Shukla, K.,

(2000). Theoretical model of thermal diffusion factors in multicomponent mixtures, *AIChE Journal: Fluid Mechanics and Transport Phenomenon*, vol. 46(5), pp.892-900

Fu W. S., Shieh W. J., (1992). A study of thermal convection in an enclosure induced simultaneously by gravity and vibration, *Int. J. Heat Mass Transfer*, vol. 35(7), pp1695-1710

Gershuni, G. Z., Lyubimov, D.V., (1998). *Thermal vibrational convection*, John Willy & Sons Ltd.: England

Guy, A. G., (1986). Prediction of thermal diffusion in binary mixtures of nonelectrolyte liquids by the use of nonequilibrium thermodynamics, *Int. J. Thermophysics*, vol.7(3), pp.563-572

Haase, R., (1969). *Thermodynamics of Irreversible Processes*, Addison Wesley

Hirata K., Sasaki T., Tanigawa H., (2001). Vibrational effects on convection in a square cavity at zero gravity, *J. Fluid Mech*., vol. 445, pp.327-344

Kempers, L.J.T.M., (1989). A thermodynamic theory of the Soret effect in a multicomponent liquid, *J. Chemical Physics*, vol. 90(11), pp.6541-6548

Kempers, L.J.T.M., (2001). A comprehensive thermodynamic theory of the Soret effect in a multicomponent gas, liquid, or solid, J. Chemical Physics, vol. 115(14), pp. 6330-6341

Kincaid J. M., López de Haro M., Cohen E.G.D., (1983). The Enskog theory for multicomponent mixtures II: Mutual diffusion, *J. Chemical Physics*, vol. 79(9), pp.4509-4521

Kozlov V.G. and Selin N.V., (2006), Pendulum Thermal Vibrational Convection in a Liquid Layer with Internal Heat Generation, FDMP: Fluid Dynamics and Materials Processing, Vol. 2, No. 2, pp. 107-118.

Lappa M., (2005), Review: Possible strategies for the control and stabilization of Marangoni flow in laterally heated floating zones, FDMP: Fluid Dynamics and Materials Processing, Vol. 1, No. 2, pp.171-188.

Lizée A., Alexander J.I.D., (1997). Chaotic thermovibrational flow in a laterally heated cavity, *Physical Review E*, vol. 56(4), pp.4152-4156

López de Haro M., Cohen, E. G. D., Kincaid, J. M., (1983). The Enskog theory for multicomponent mixtures. I. Linear transport theory, *Journal of Chemical Physics,* vol. 78(5), 2746-2759

Monti, R., Savino R., Lappa M., (2001). On the convective disturbances induced by g-jitters on the space station, *Acta Astronautica,* vol. 48(5-12), pp 603-615

Monti, R., Patterna, D., Savino R., (2002). Counter-measures to migrate residual-g effects on microgravity experiments on the space station, *Acta Astronautica,* vol. 50(4), pp 209-216

Mortimer, R. G., Eyring, H., (1980). Elementary transition state theory of the Soret and Dufour effects, *Proceedings of the National Academy of Sciences of the United States of America-Physical Sciences*, vol. 77, 1728-1731

Okano Y., Ishii A., Miyashita H., Minakuchi H., and Dost S., (2006), A numerical study of controlling the g-jitter induced convection in the solution of a crystal growth crucible under microgravity, FDMP: Fluid Dynamics and Materials Processing, Vol. 2, No. 4, pp. 261-270.

Peng, D.Y., Robinson, D.B., (1976). A new two-constant equation of state, *Industrial and Engineering Chemistry Fundamental*, vol.15, pp.59-64

Rutherford, W. M., Roof, J. G., (1959). Thermal Diffusion in Methane-n-Butane Mixtures in the Critical Region, *J. Physical Chemistry*, vol. 63(9), pp.1506-1511

Savino R., (2002). Residual-g and g-jitter effects on the measurement of thermophysical properties in microgravity, *Advanced Space Research*, vol. 29(4), pp 559-568

Savino R., Lappa M., (2003). Assessment of thermovibrational theory: application to g-jitter on the Space Station, *J. Spacecraft and Rockets*, vol. 40(2), pp.201-210

Shu Y., Li B.Q., (2005). Ramaprian B.R., Convection in modulated thermal gradients and gravity: experimental measurements and numerical simulations, *Int. J. Heat Mass Transfer*, vol. 48(1), pp.145-160

Twu, C.H., Coon, J.E., (1995). Cunningham, J.R., A new generalized alpha function for a cubic equation of state part 1. Peng–Robinson equation, *Fluid Phase Equilibrium*, vol. 105(1), pp.49-59

Semma E.A., El Ganaoui M., Timchenko V., and Leonardi E., (2006), Some Thermal Modulation Effects on Directional Solidification, FDMP: Fluid Dynamics and Materials Processing, Vol. 2, No. 3, pp. 191-202.

Shukla K., Firoozabadi A., (1998). A new model of thermal diffusion coefficients in binary hydrocarbon mixtures, *Ind. Engrg. Chem. Res.*, vol. 37(8), pp.3331 -3342

Yan Y., Shevtsova V., Saghir, M.Z., (2005). Numerical study of low frequency g-jitter effect on thermal diffusion, *FDMP: Fluid Dynamics and Materials Processing*, vol. 1, no. 4, pp315-328

Yan Y., Adimoolam C., Saghir, M.Z., (2006). Double diffusion convection under sinusoidal modulations of low frequency vibrations, *57th International Astronautical Congress*, Spain, October, IAC-06-A2.2.02